Journal of Volcanology and Geothermal Research 427 (2022) 107572

Contents lists available at ScienceDirect

Journal of Volcanology and Geothermal Research

journal homepage: www.journals.elsevier.com/journal-of-volcanology-and-geothermal-research

Multiyear temporal variation of *b*-values at Alaskan volcanoes: The synergetic influence of stress and material heterogeneity

K.I. Konstantinou

Dept of Earth Sciences, National Central University, Jhongli 320, Taiwan

ARTICLE INFO

Keywords:
b-value
Seismicity
Volcanoes
Alaska
Stress
Heterogeneity

ABSTRACT

Changes in seismicity parameters is often utilized as a tool for forecasting eruptive activity at volcanoes worldwide. One of these parameters is the slope of the Gutenberg-Richter law, known as the *b*-value, whose temporal variation is studied here as an indicator of volcanic activity. Four Alaskan volcanoes (Makushin, Martin, Redoubt, Spurr) were selected in order to reconstruct the *b*-value variation over a multiyear period ($\geq$ 25 years). The magnitude of completeness and the *b*-value were estimated using a sliding window for each earthquake catalog, while bootstrap uncertainties were estimated for each window. The size of the analysis window was selected by applying the Magnitude Bandwidth Criterion (MBC) that maximizes the number of windows with magnitude bandwidth larger than 2.0 in the complete part of the catalog. All four volcanoes exhibit decreasing *b*-values before unrest and eruptions, while maximum *b*-values exceed 1.0 only at Redoubt and Spurr. Previously published laboratory experiments on volcanic rock deformation and failure suggest that the decrease in *b*-value is a result of increased stress that may stem either from magma intrusions or from exsolution of volatiles. On the other hand, whether the *b*-value at each volcano will exceed 1.0 or not, is also determined by the degree of material heterogeneity.

1. Introduction

Volcanoes along subduction zones are responsible for the largest fraction of explosive activity worldwide and also constitute a source of volcanic hazards for the people living near them (Wilson and Parfitt, 2008). The Aleutian arc is formed by the subduction of the Pacific plate beneath the North American plate and hosts a chain of 142 Quaternary volcanic centers, 32 of which (Fig. 1) have been active in historical times and are seismically monitored (Tibaldi and Bonali, 2017; Power et al., 2020). Volcanism along the Aleutian arc is believed to be affected by the increasing obliquity of the Pacific plate movement as well as the amount of H_2O that is being released from the downgoing slab, resulting in the central part of the arc being the most active (Buurman et al., 2014; Wei et al., 2021). Despite the fact that the population density along the Aleutian islands is low, eruptive activity can still pose a threat to oil industry infrastructure and to commercial flights that frequently traverse this area. An increase in seismicity is considered as a potential precursor to eruptive activity (White and McCausland, 2019) and several eruptions at Alaskan volcanoes have been preceded by changes in seismicity rates, providing the means for their successful forecasting (Pesicek et al., 2018). It is therefore clear that the study of the temporal variation of seismicity and its properties can yield useful information about the status of a volcano and may help forecast eruptions.

Seismicity at active volcanoes is usually characterized by small-magnitude earthquakes occurring in swarms, whose frequency of occurrence *N* is related to their magnitude *M* by the Gutenberg-Richter (or Ishimoto-Iida) law (Ishimoto and Iida, 1939; Gutenberg and Richter, 1944) such that

$$logN(M) = a - bM \quad (1)$$

The slope of this line, widely known as the *b*-value, represents the relative proportion between larger and smaller events in an earthquake population. Laboratory experiments and observational evidence has shown that the *b*-value has an inverse relationship with stress, while other factors that may also affect *b*-values include material heterogeneity, pore fluid pressure and thermal gradients (Scholz, 1968; Warren and Latham, 1970; Sammonds et al., 1992; Schorlemmer et al., 2005; El-Isa and Eaton, 2014; Scholz, 2015; Goebel et al., 2017). The spatial distribution of the *b*-value has received particular attention as an efficient tool for mapping the extent of magma chambers beneath active volcanoes (Wyss et al., 1997; Wiemer et al., 1998; Murru et al., 1999; Wyss et al., 2001; Farrell et al., 2009; Chiba and Shimizu, 2018). It has

E-mail address: kkonst@ncu.edu.tw.

https://doi.org/10.1016/j.jvolgeores.2022.107572
Received 30 January 2022; Received in revised form 26 April 2022; Accepted 3 May 2022
Available online 8 May 2022

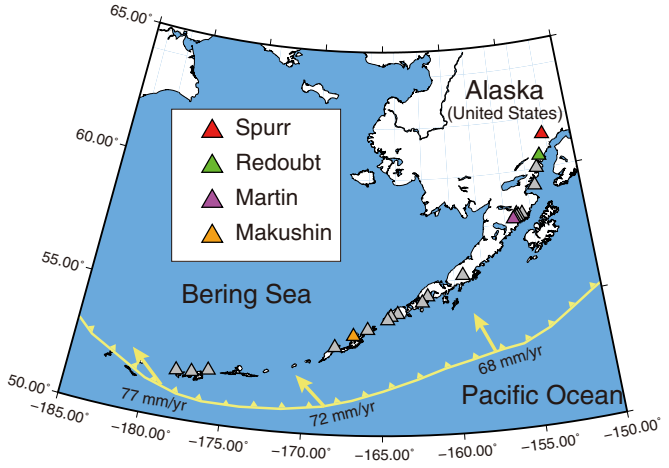

Fig. 1. Map of the Alaska peninsula and the Aleutian islands chain also depicting the subduction front as a thick yellow line. The yellow arrows show the direction of the plate convergence and the numbers indicate the convergence rate (Buurman et al., 2014 and references therein). Grey triangles represent active volcanoes that are monitored by AVO using a local seismic network (Power et al., 2020) and the colored triangles shown in the legend are the ones selected for analysis in this study. (For interpretation of the references to colour in this figure legend, the reader is referred to the web version of this article.)

been found that magma chambers are usually surrounded by a halo of high (> 1.0) *b*-values that reflect the increased density of small cracks due to repeated intrusion activity. On the other hand, the temporal variation of *b*-values at active volcanoes is a subject that has been studied in less detail, even though it could be used as another indicator of impending eruptive activity and could be incorporated into volcanic alert schemes.

This work utilizes earthquake catalogs of Alaskan volcanoes that span several years in order to study the temporal variation of the *b*-value during unrest as well as during eruptive periods. The motivation behind such a study is twofold: first, considerable biases exist in the estimation of *b*-values hence it is important to carefully examine how these influence the temporal variation; second, to relate the estimated *b*-values with the results of previous laboratory experiments that investigated the mechanical behavior and failure of volcanic rocks. The analysis begins with a description of the earthquake catalogs and the selection of a number of active volcanoes that contain a sufficient number of events spanning several years. A novel criterion for selecting the window size for such an analysis is introduced and results are then presented for each volcano. The different biases in the calculation of *b*-values are then considered and this is followed by a discussion focused on the physical interpretation of *b*-value variation.

2. Catalog data

The Alaska Volcano Observatory (hereafter called AVO) is the agency responsible for monitoring the volcanoes along the Alaska peninsula and the Aleutian islands, as well as for issuing alerts for any impending eruption (Cameron et al., 2018). AVO operates a seismic network that initially consisted of 29 stations and by now has expanded to 217 stations that provide real-time monitoring for 32 active volcanoes (see also Fig. 1) (Power et al., 2020). Since the beginning of seismic monitoring in 1988, AVO has routinely picked and located volcanic seismicity, including the calculation for each event of local or duration magnitude. This has resulted in a catalog that contains more than 120,000 earthquakes consisting of volcano-tectonic, long-period and explosion events that span a period from October 1989 up to present time. Changes in seismic instrumentation and data acquisition over the years, along with advances in seismological software, have put forward

Table 1
List of volcanoes whose seismicity has been used to infer the temporal variation of *b*-values. The columns *R* and *H* represent the radius and maximum hypocentral depth respectively that define the horizontal and vertical extent of the selected seismicity (see Buurman et al., 2014). Neq is the total number of earthquakes found at each volcano.

Volcano	Lon (°W)	Lat (°N)	Elevation (m)	*R* (km)	*H* (km)	Neq
Makushin	−166.923	53.891	1800	12	12	4474
Martin	−155.361	58.172	1863	<3	12	6754
Redoubt	−152.742	60.485	3108	8	12	8951
Spurr	−152.251	61.299	3374	10	40	9280

the need for increasing the consistency of the catalog in terms of earthquake hypocenters and magnitudes. This data reprocessing involved the relocation of hypocenters between 1989 and 2012 using Hypoinverse and utilizing local velocity models whenever possible, as well as the recalculation of magnitudes for events in the period from early 2011 to the end of 2017 (Power et al., 2019). A comparison of the new and old locations showed that the standard deviations of horizontal and vertical shifts were 1.8 km and 2.4 km respectively, while the corresponding standard deviation for magnitudes was equal to 0.31 units (see Power et al., 2019).

For the purpose of this study a number of criteria was established in order to select volcanoes that would be suitable for the estimation and temporal analysis of *b*-values. The first criterion had to do with the existence of a local seismic network around the volcano that would insure the relatively good quality of the earthquake locations. The second criterion is that each selected volcano should exhibit significant volcano-tectonic seismicity (at least 4000 events) related to either unrest and/or eruptive activity. The third one requires that the recorded seismicity spans at least 25 years so that the long-term variation of *b*-values can also be studied. Four Alaskan volcanoes were found to be in accordance with these criteria namely Makushin, Martin, Redoubt and Spurr (cf. Fig. 1). A separate earthquake catalog for each volcano was compiled by defining a search radius *R* and maximum hypocentral depth *H* according to values suggested by Buurman et al. (2014) as representative for these volcanoes (Table 1). As already mentioned above, the reprocessed AVO catalog covers the period from October 1989 until the end of December 2017, therefore the seismicity from January 2018 up to the end of July 2021 was obtained from the online ANSS database. Fig. 2 shows the temporal variation of hypocentral depth for each of the four selected volcanoes. Makushin and Martin exhibit an apparently stable seismicity over the last two decades, even though both of them have experienced periods of unrest. The seismicity at Redoubt appears more clustered in time due to the fact that the volcano erupted in 1989 and again in 2009, while at Spurr the seismicity becomes significantly deeper during 1992 and 2005 as a result of an eruption and unrest period respectively. At all 4 volcanoes the majority of the events have a magnitude below 3.0 representing swarm microseismicity as it would be expected in volcanic areas (e.g., Roman and Cashman, 2006).

3. Methodology

3.1. Estimation of b-values and completeness magnitude

Marzocchi and Sandri (2003) reviewed the different methods that have been employed in the literature for the estimation of *b*-values. Perhaps the most popular of these methods is based on the maximum likelihood technique, hereafter referred to as the Aki-Utsu method (Aki, 1965; Utsu, 1965). The *b*-value is estimated by taking into account that the earthquake magnitudes are not continuous variables, but are accurate only to a single digit. The equation to estimate the *b*-value using the Aki-Utsu formulation is

$$b_{AU} = \frac{loge}{< M > -(M_c - \delta M/2)} \quad (2)$$

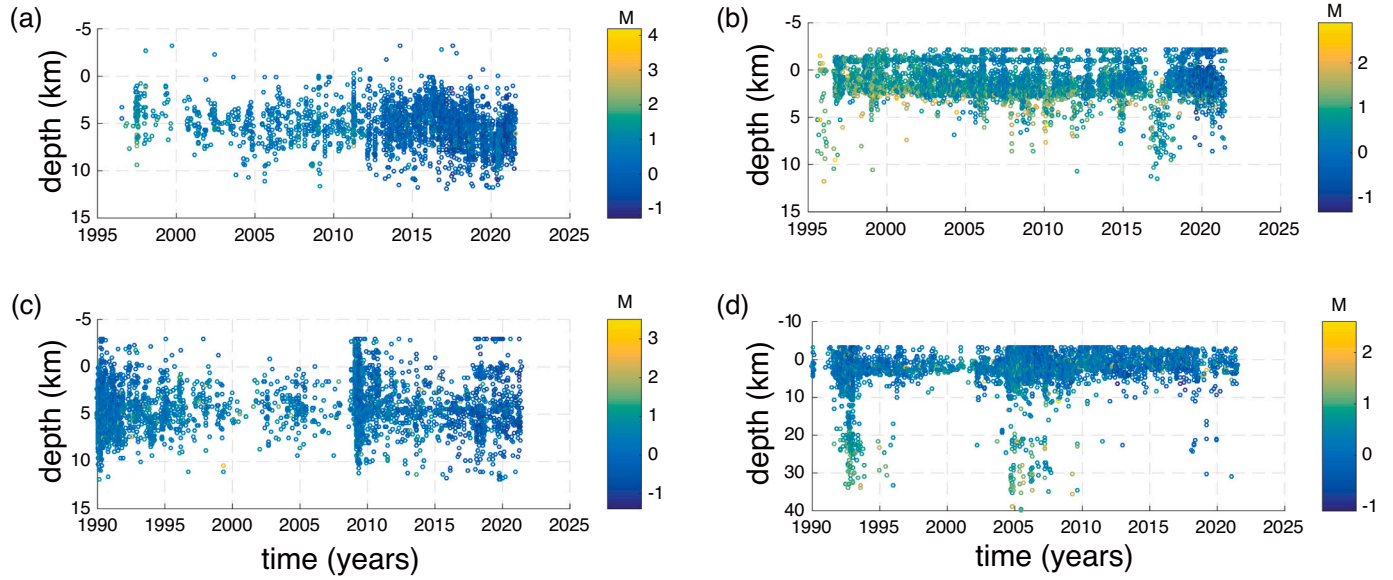

Fig. 2. Plots of hypocentral depth versus time for the seismicity recorded at (a) Makushin, (b) Martin, (c) Redoubt and (d) Spurr volcano. The local (or duration) magnitude of each event is indicated by the colour scale at the right hand side of each plot.

where e is the base of natural logarithms, $<M>$ is the mean magnitude, M_c is the completeness magnitude of the catalog and δM is the amount of binning which is equal to 0.1 units for catalogs in the instrumental era.

The estimation of b-values requires that the completeness magnitude of the earthquake catalog is known, or at least that it can be estimated. The completeness magnitude can be defined as the smallest magnitude at which all earthquakes are detected by the seismic network (Wiemer and Wyss, 2000). Several techniques have been proposed for the estimation of M_c and the strengths and weaknesses of each of them were described in Woessner and Wiemer (2005) and more recently in Mignan and Woessner (2012). More specifically, the three most widely utilized techniques for estimating M_c are the Maximum Curvature (MaxC), Goodness-of-Fit Test (GFT), and b-Value Stability (bVS) respectively. MaxC estimates the completeness magnitude by finding the frequency-magnitude bin with the largest number of events, relying heavily on the assumption that the non-cumulative frequency-magnitude distribution has a sharp peak. GFT varies the value of M_c and calculates each time different a and b values that form a frequency-magnitude distribution that is compared to the observed one. The value of M_c where the residuals between the calculated and the observed distribution falls within the 90% confidence interval is considered as the sought completeness magnitude. The bVS technique also varies M_c and calculates each time the corresponding b-value, assuming that for M_c close to the true completeness magnitude the b-value will be stable.

Roberts et al. (2015) have tested the performance of the three aforementioned techniques using synthetic earthquake catalogs that mimicked some of the characteristics found in volcanic seismicity such as sharp or broad-peaked distributions, variable catalog sizes (50–5000 events), and earthquake populations with high b-values (b= 1.0 or b= 2.0). The results of these tests showed that the bVS technique performed better than the other two in reproducing the correct M_c and b-value within the 95% confidence limits. The number of events in the complete part of the catalog N_c seemed to have a strong effect on the results with the authors suggesting that $N_c \geq$ 200 is a necessary condition for obtaining reliable results. Following Roberts et al. (2015), the bVS technique is also employed in this work for the estimation of the completeness magnitude. An analysis of temporal variation necessitates the use of a sliding window where the b-value will be estimated as a function of time. This poses the question of whether the completeness magnitude should be estimated for the whole catalog, or for each individual window. Considering that M_c may vary strongly as a function of time, the bVS technique is applied in order to estimate M_c for each time window. The next section describes how to choose objectively the size of such a window by using a novel criterion for this task.

3.2. Selection of window size and estimation of uncertainties

The size of the sliding window used for the temporal analysis of an earthquake catalog can be defined either in terms of time duration, or as the number of events that each window must contain. The latter approach is what is actually employed in almost all studies of b-value estimation, for the reason that this estimation is sensitive to the number of events used, with smaller sizes (50–100 events) being more susceptible to produce biased results (Roberts et al., 2015; Nava et al., 2016; Marzocchi et al., 2019). Another source of bias that is linked to the window size is that of magnitude bandwidth. Magnitude bandwidth ΔM is defined as the difference between the largest magnitude M_{up} and minimum magnitude M_{min} that exist in the complete part of an earthquake catalog. Marzocchi et al. (2019) showed that when ΔM= 3.0 the bias in the estimated b-value is negligible, increasing to about 3% when the bandwidth becomes 2.0, while the bias increases exponentially for smaller magnitude bandwidths. This source of bias is particularly relevant for volcanic seismicity since M_{up} seldom exceeds 3.0 (see Fig. 2) and M_{min} is strongly influenced by the temporal and spatial heterogeneity of the completeness magnitude.

The approach taken here is to select the window size in a way that ΔM will be maximized while at the same time the window duration will be as short as possible. The first step in order to do this is to assume different window sizes and for all windows of a particular size estimate M_c, ΔM and window duration. It is then possible to find for each particular window size the number of windows where ΔM is larger or equal to a value m and also calculate the median duration for these windows. After this the following percentage can be calculated

$$W = \left[\frac{N_w(\Delta M \geq m)}{N} - \frac{\widetilde{T}_w}{T}\right] \times 100\% \quad (3)$$

where $N_w(\Delta M \geq m)$ is the number of windows with $\Delta M \geq m$ for a particular window size, $\widetilde{T}_w$ is the median duration of these windows for a particular window size, N is the total number of windows and T is the

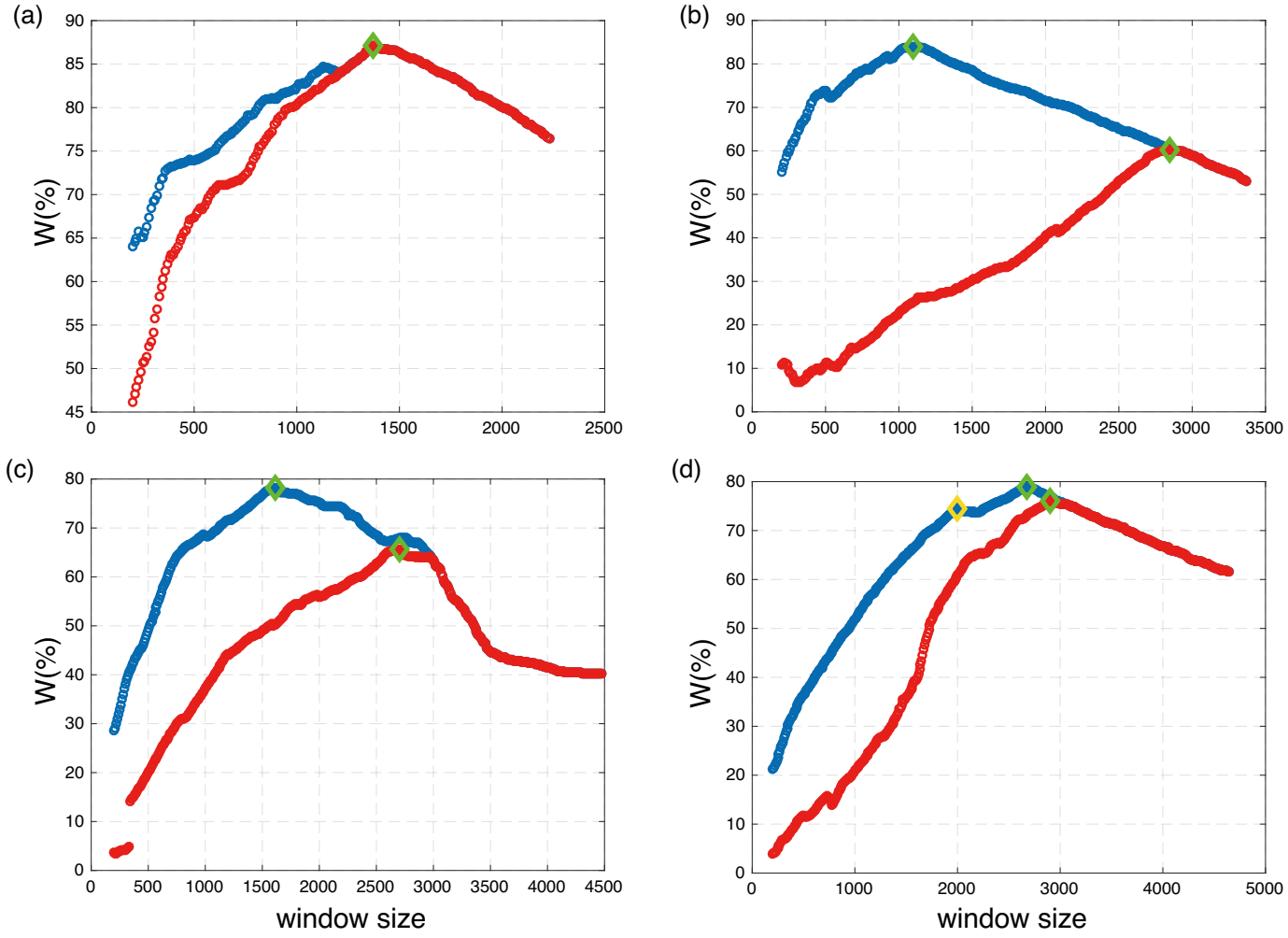

Fig. 3. Diagrams showing the resulting curves after the application of MBC to the four selected volcanoes: (a) Makushin, (b) Martin, (c) Redoubt, and (d) Spurr. The blue curve corresponds to m = 2.0 and the red curve to m = 2.5. The green diamonds highlight the global maximum of each curve, while the yellow diamond in (d) represents the first maximum that corresponds to the window size of 2000 events chosen for Spurr (see text for more details). (For interpretation of the references to colour in this figure legend, the reader is referred to the web version of this article.)

total duration of the earthquake catalog. When the percentage W attains its maximum value, the majority of windows has $\Delta M \geq m$ and the shortest possible duration. A plot of W versus the window size would then produce a curve that can be used to choose the optimum size as the one that maximizes W. Hereafter, this method of selecting the window size will be referred to as the Magnitude Bandwidth Criterion (MBC). MBC was applied to the earthquake catalogs of the four Alaskan volcanoes by defining a range of window sizes from a starting value of 200 events, incremented each time by 10 events, until it reaches a value equal to half of the number of events contained in the catalog. Fig. 3 shows the curves for m= 2 and 2.5 at each volcano along with symbols marking the different points where a maximum occurs. At Makushin both curves exhibit a global maximum at a window size of 1370 events, while for Martin and Redoubt the optimum window size (1100 and 1610 events respectively) coincides with the global maximum of the curve with m= 2.0. At Spurr both curves exhibit a global maximum near a window size of 2600–3000 events, which would truncate significantly the b-value time series. In order to avoid such a truncation, a window size of 2000 events was chosen that corresponds to the first maximum of the curve with m= 2.0 and has a difference in W of less than 5% relative to the global maximum.

The completeness magnitude and b-values are estimated as a function of time for a sliding window shifted each time by 1 event as implemented in similar studies previously (e.g., Gulia et al., 2016). Following Roberts et al. (2015) b-values estimated with less than 200 events above the completeness magnitude are rejected, a constraint that is relatively easy to satisfy since the window size ranges from 1370 events at Makushin to 2000 events at Spurr. The last but necessary step in this analysis is the estimation of uncertainties both for the completeness magnitudes and the b-values. This is accomplished by creating bootstrap samples for each window and estimate for each one of them M_c and the b-value. The uncertainty of the b-value for the jth window is then given by the standard error

$$\delta b_j = \sqrt{\frac{1}{n-1}\sum_{i=1}^{n}\left(b_i - < b_j >\right)^2} \quad (4)$$

where n is the number of bootstrap samples, b_i is the b-value of the ith bootstrap sample and $<b_j>$ is the average b-value of all bootstrap samples for the jth window. In order to obtain meaningful uncertainties the number n was set equal to 1000. The uncertainty of completeness magnitude for each window was calculated in the same way as for the b-value.

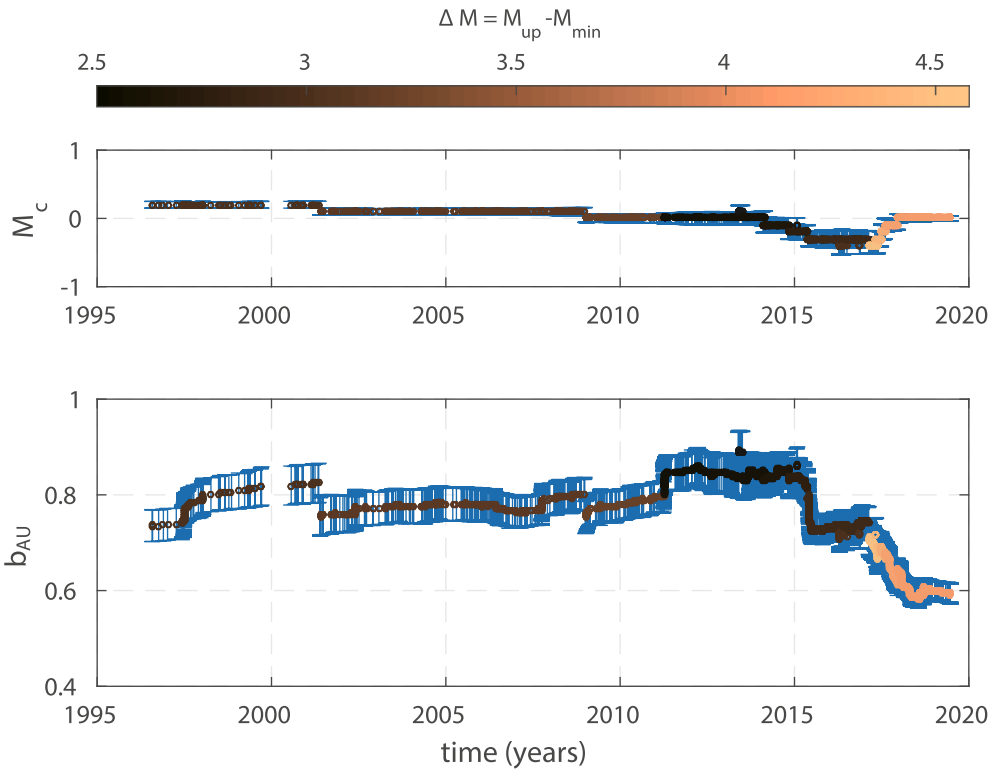

Fig. 4. Evolution of completeness magnitude Mc and *b*-value as a function of time for the seismicity recorded at Makushin volcano. Each circle represents a time window over which the two quantities are estimated. The colour of each circle follows the scale at the top and signifies the magnitude bandwidth of each window. The blue error bars indicate bootstrap uncertainties for each window. (For interpretation of the references to colour in this figure legend, the reader is referred to the web version of this article.)

4. Results

4.1. Makushin

Makushin volcano has an elevation of 1800 m and lies on northern Unalaska island near the town of Unalaska, while it is also close to oil storage facilities. During the Holocene the volcano experienced frequent explosive eruptions (VEI 1–5) with 13 of these occurring after 1768 BCE and the most recent one taking place in January 1995 (GVP, 1995a). Travel time as well as attenuation tomography have revealed that the upper 5 km of the crust beneath Makushin exhibit high P-wave velocities and low attenuation, suggesting the presence of solidified intrusions (Syracuse et al., 2015; Lanza et al., 2020). A low velocity body was imaged in the depth range of 5–7 km that can be interpreted as a shallow magma chamber filled with mafic magma. This low velocity body also coincides with an area of high *b*-values and inflation sources observed using InSAR (Bridges and Gao, 2006). Makushin has experienced two periods of unrest, the first of which occurred during 30 May-5 June 2001 and was accompanied by microseismicity ($M<$ 1.5) but without any observed activity at the surface (GVP, 2001). The second period occurred from 10 June-8 September 2020 and involved increased seismicity accompanied by moderate events (M ~4.1) as well as minor steaming from the summit fumaroles (GVP, 2020).

Fig. 4 shows the temporal variation of the magnitude of completeness and the corresponding *b*-values at Makushin since early 1996. Except from the bootstrap uncertainties of both quantities, the diagrams also depict the magnitude bandwidth of each window. Such a plot has two main advantages: first, it makes easier to detect how changes in M_c can affect the estimated *b*-value, and second, it indicates which parts of either time series may be biased due to ΔM being smaller than 2. Completeness magnitude appears to change very little until 2015 when it becomes negative, increasing again progressively after 2017. The *b*-value varies slowly from being slightly above 0.7 in 1996 to 0.8 in 2010, followed by a period of further increase to a value close to 0.9 until 2015, when it gradually decreases to 0.6 after 2018. It can be seen that the change in M_c after 2015 has an effect on the *b*-value variation, since both quantities exhibit a plateau between 2015 and 2017. However, after 2017 M_c increases back to zero while the *b*-value continues to decrease and stabilizes to a value of about 0.6. This decrease seems to be jointly related to the occurrence of moderate events and to the coeval variation of completeness magnitude. Recently, Lanza et al. (2022) argued that the 2020 seismic unrest had a magmatic origin based on fault plane solutions of volcano-tectonic earthquakes and Coulomb stress modeling. The authors found that P-axes orientations indicated significant deviations from the regional stress orientations and that the stress field generated by the swarm could have been caused by an inflating dike.

4.2. Martin

The Katmai volcano group consists of five closely spaced volcanoes that have been active during the Holocene, namely Katmai, Novarupta, Trident, Martin and Mageik. More specifically, Martin volcano has had four eruptions in this period, the oldest of which probably occurred in 1750 BCE and the most recent in 1953, even though not much is known about the size and style of these eruptions. Martin has also exhibited two periods of unrest, the first starting in 1995 which involved observations of large steam plumes rising from its summit crater, followed in December 1998 and May–July 1999 by increased seismic activity (GVP, 1995b, 2012). The second period of unrest started in January 2006 with a swarm of volcano-tectonic events that was repeated during May–June 2007 and again in December 2008 (GVP, 2012). These swarms were not accompanied by long-period seismicity or volcanic tremor, while there were no observations of ice melting due to shallow thermal anomalies. Interestingly, seismic tomography along the Katmai volcano group has imaged a low-velocity body beneath the neighboring Mageik volcano, but did not detect any low-velocity anomalies beneath Martin (Murphy et al., 2014). Based on a study of the stress field derived from inversion of earthquake focal mechanisms, Moran (2003) concluded that the seismogenic stress field beneath Martin is influenced by long-term edifice loading and by repeated emplacement of small magma bodies.

The temporal variation of M_c and *b*-value for Martin volcano can be

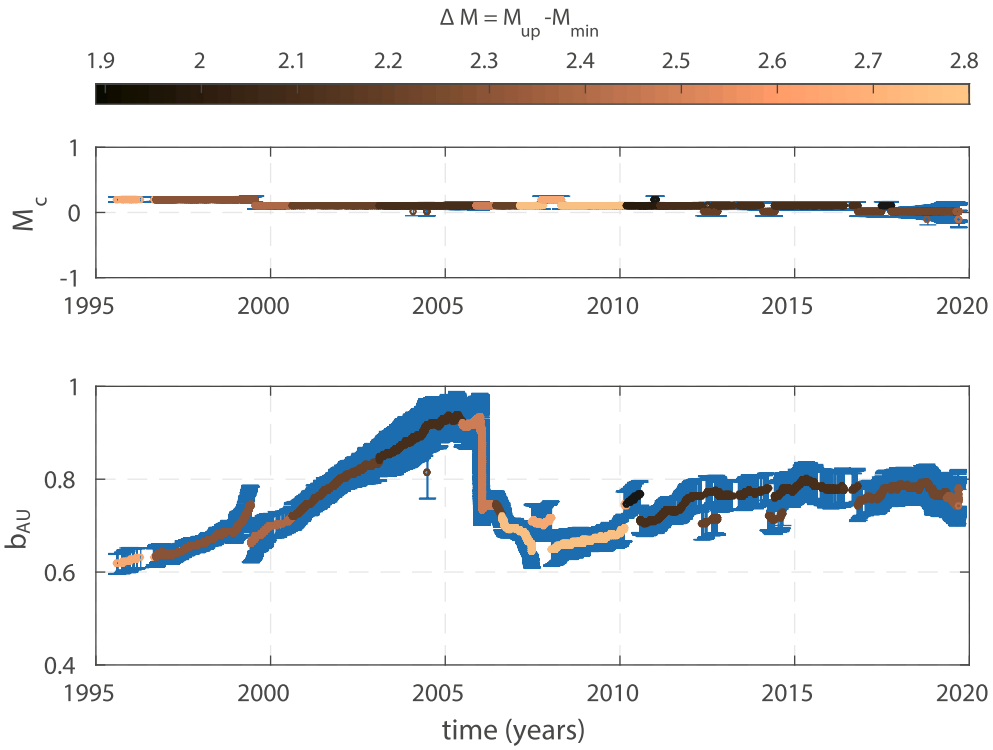

Fig. 5. Evolution of completeness magnitude Mc and *b*-value as a function of time for the seismicity recorded at Martin volcano. All other symbols are the same as in Fig. 4.

seen in Fig. 5 plotted in the same format as in the case of Makushin. The completeness magnitude varies little during the period covered by the catalog with a few upward or downward shifts around zero, however, these shifts involve only a small number of windows and do not affect the general trend. The *b*-value starts from 0.6 in 1995 and gradually increases to more than 0.7 in the middle of 1999 dropping slightly afterwards, mirroring in this way a similar change in M_c. The increase in *b*-value grows continuously after the year 2000 when it reaches a maximum close to 1.0 after 2005, which is also the maximum value for the whole period under study. From the end of 2005 the *b*-value decreases rapidly and reaches a first minimum at 0.7 in 2006 while after that it continues to drop to a second minimum (~0.6) in the middle of 2007. After 2007 the *b*-value increases slowly and stabilizes to a value close to 0.8 for the remaining period. It is interesting to note the good correlation between the maximum and minimum *b*-values and the periods of unrest at Martin as described previously. Even though it is not known whether magma emplacement was involved in the 1995–1999 unrest, the unrest that started in early 2006 was likely caused by a magmatic intrusion. This view is supported by the stress field induced by the earthquake swarm (O'Brien et al., 2012) and geochemical observations of SO_2/H_2S ratio that indicate a magmatic source (Lopez et al., 2017).

4.3. Redoubt

Redoubt is an andesitic stratovolcano that is located to the west of Cook inlet and is 180 km from Anchorage, the largest city in Alaska. There were numerous confirmed eruptions of Redoubt during the Holocene, with the earliest occurring in 9310 BCE, while the two latest ones in 1989 and 2009 (both having VEI = 3) were the first to be observed using modern instrumentation. The 1989 eruption started in December with a vigorous swarm of volcano-tectonic events and culminated in April 1990 with a lava dome extrusion, followed by vulcanian explosions until June 1990 (Power et al., 2013 and references therein). Redoubt remained dormant for almost 20 years until edifice inflation was first observed in May 2008 and was later followed by bursts of volcanic tremor in September 2008 and deep (28–32 km) long-period earthquakes in December of the same year. Swarms of volcano-tectonic events continued occurring in January up to March 2009 when lava dome extrusion started and was accompanied by several explosions with activity waning by early July 2009 (Bull and Buurman, 2013; Buurman et al., 2013). Available tomographic images at Redoubt have sufficient resolution only down to 5 km depth delineating no low-velocity bodies, however, they do reveal an increase of the Vp/Vs ratio from 1.8 to a value of 2.0 after the 2009 eruption (Kasatkina et al., 2014; Hong et al., 2014).

Fig. 6 shows the temporal variation of M_c and *b*-values at Redoubt volcano truncated up to the end of April 2009 due to the size of the selected window (see section 3.2 and Fig. 3). The completeness magnitude exhibits a small but gradual increase from about the end of 1991 until the end of 2008, which likely reflects the fact that the alert status was lowered once the volcano became dormant again. This increase in M_c also affects the *b*-value variation, since there are two step-like shifts in 1992 and 1999 that appear to break the continuity of the time series. Aside from these features, the *b*-value is equal to 1.1 in December 1989 decreasing to 1.0 in April 1990 and further decreasing close to 0.9 in the middle of 1992. The two step-like shifts divide the *b*-value variation into two periods, namely 1992–1999 and 1999–2009, where it attains stable values slightly below and above 1.0 respectively. The *b*-value variation during the period covering the 2009 eruption is given at the lower panel of Fig. 6, where it can be seen that initially the *b*-value was close to 1.2 without exhibiting any significant fluctuation. After this the *b*-value started decreasing rapidly reaching a value close to 0.6, subsequently increasing again to 0.9 and slowly reaching 1.0 towards the end. The windows when the *b*-value became minimum include the occurrence of a strong swarm of volcano-tectonic events that occurred just before the extrusion of the lava dome. This swarm was interpreted by Buurman et al. (2013) as the result of crack opening ahead of the moving magma.

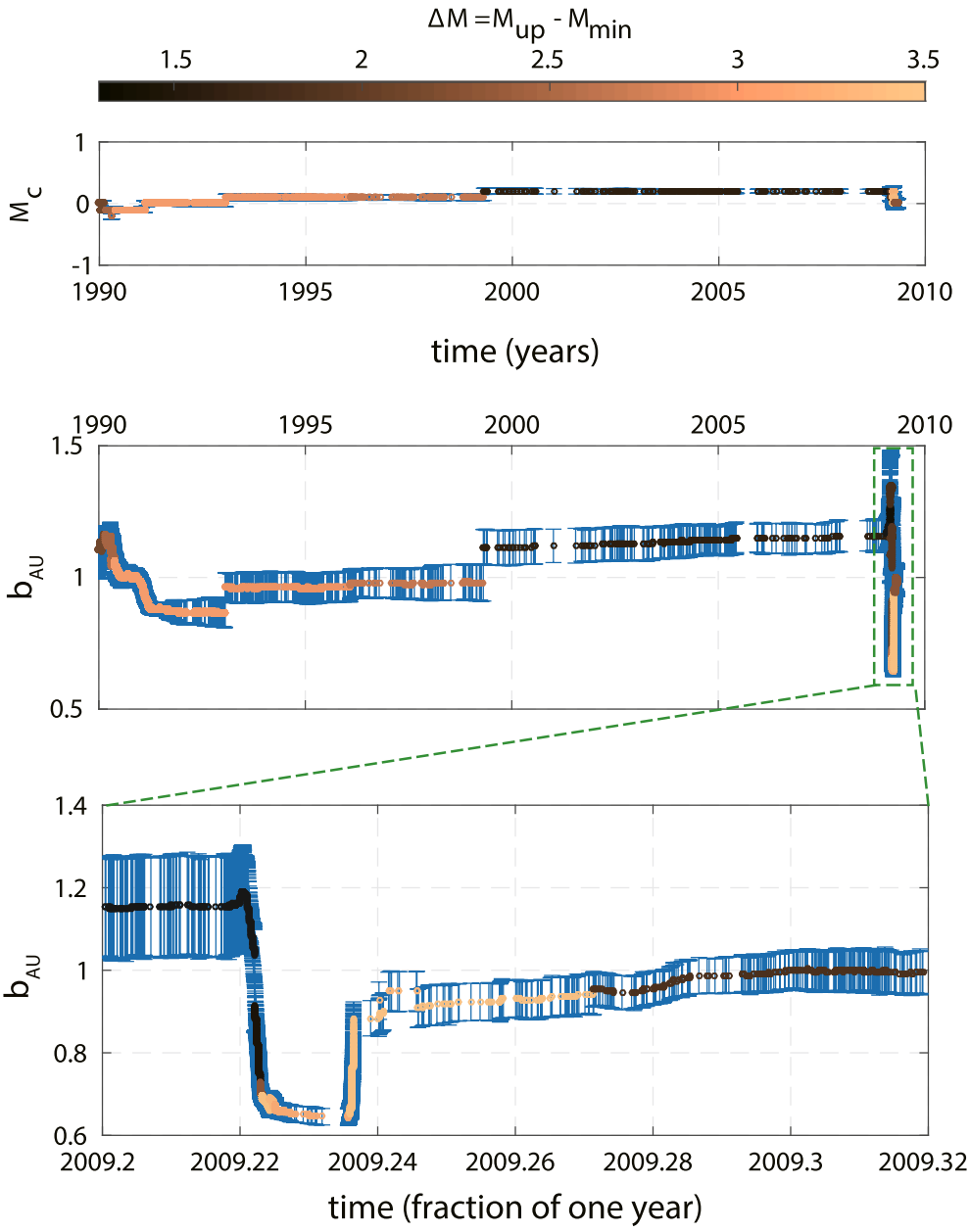

Fig. 6. Evolution of completeness magnitude Mc and *b*-value as a function of time for the seismicity recorded at Redoubt volcano. The lower panel magnifies the *b*-value variation during the 2009 eruption. All other symbols are the same as in Fig. 4.

4.4. Spurr

Spurr is the highest volcano in the Aleutian arc, reaching an elevation of 3374 m above sea level and is also located about 130 km west of the city of Anchorage. Its eruption record includes several confirmed eruptions in the Holocene, while the volcano erupted twice in the 20th century, first on 9 July 1953 and again on 27 June 1992 with a VEI equal to 4 for both eruptions. The 1992 eruption was preceded 9 months earlier by intense seismicity and by the occurrence of volcanic tremor due to a magma intrusion 5–15 km beneath the volcano (Power et al., 2002). Volcano-tectonic earthquakes continued to occur in swarms after the onset of the eruption and also after September 1992 when eruptive activity ceased. Spurr remained dormant until early 2004 when swarms of volcano-tectonic and long-period earthquakes started being recorded, reaching a peak between July and November 2004. Activity continued throughout 2005 until early 2006, however, the number of earthquakes had decreased relative to the activity in 2004. This unrest was accompanied by ice melting, flux of CO_2 and SO_2 gases (Doukas and McGee, 2007), as well as an inflation of 5 cm detected by InSAR (Lu and Dzurisin, 2014). Time-lapse seismic tomography from 1992 until 2012 revealed that the cause of the unrest was the upward migration of fluids that broke the brittle cover of the ductile reservoir which lies at 5–10 km beneath the edifice of the volcano (Kulakov et al., 2018).

As mentioned earlier the seismicity at Spurr occurs at depths down to 40 km, therefore the temporal variation of M_c and *b*-value was first estimated for all available events and then only for the shallow ($\leq$ 12 km) seismicity (Fig. 7a,b). In both cases the completeness magnitude varies slightly around zero, which allows the recovery of *b*-value variations during the eruption and unrest without the introduction of significant artifacts. When considering all events, the *b*-value appears to be initially stable above 1.0 prior to the 1992 eruption and starts decreasing by the end of 1991, reaching a minimum (~0.9) near the time of the eruption (cf. Fig. 7a). Following the eruption it started to increase again reaching 1.0 in early 1993 and it remained stable around this value until

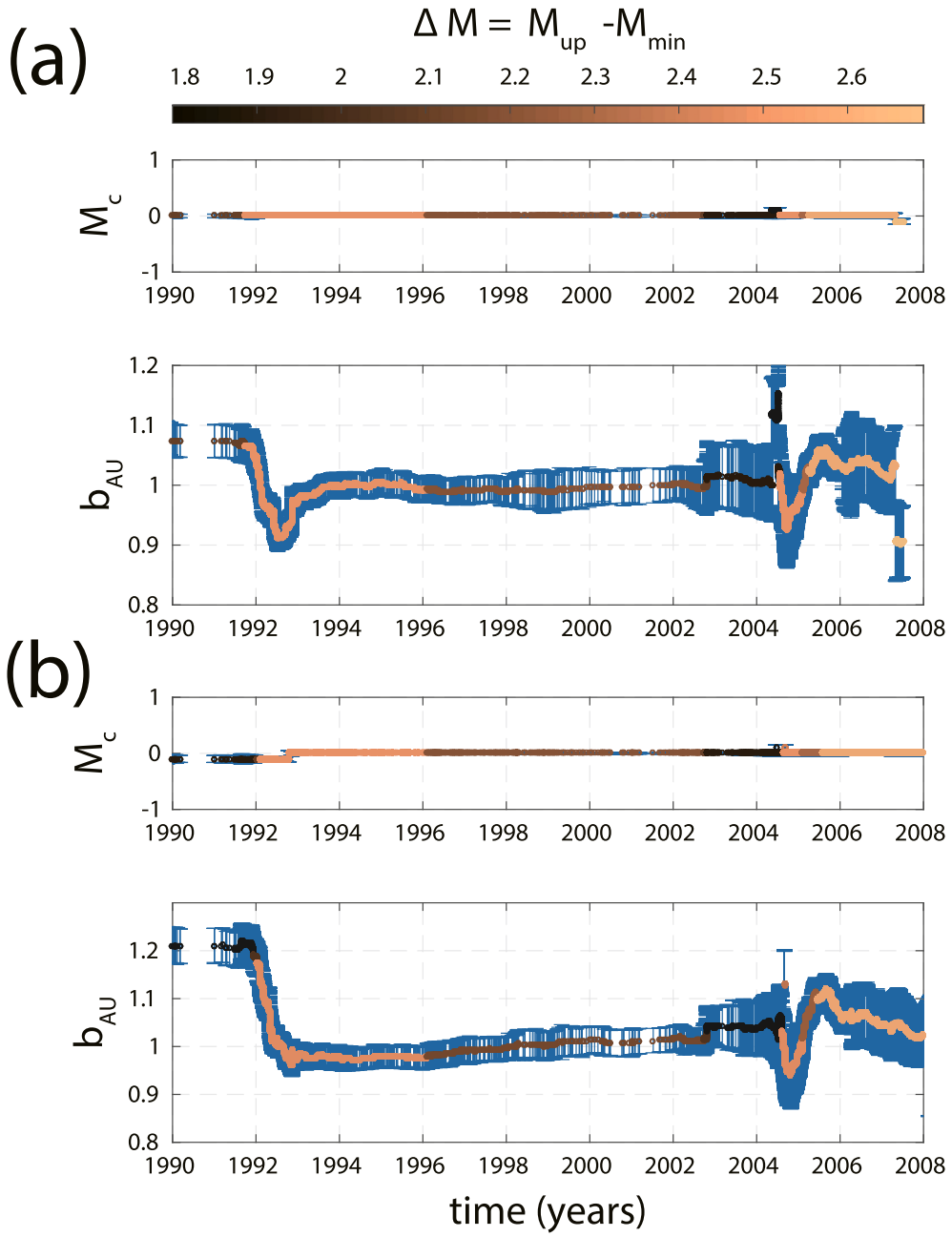

Fig. 7. Evolution of completeness magnitude Mc and *b*-value as a function of time for the seismicity recorded at Spurr volcano. Panel (a) corresponds to events up to a hypocentral depth of 40 km, and panel (b) to events with hypocentral depths shallower than 12 km. All other symbols are the same as in Fig. 4.

early 2004. Once the unrest started the *b*-value decreased quickly to a minimum around 0.9, gradually increasing in the second half of 2004 and early 2005. By the middle of 2005 the *b*-value reached a maximum (> 1.0) and subsequently fluctuated around 1.0 signifying that the unrest was essentially over. When only the shallow seismicity is considered a similar pattern appears, however, the maximum *b*-value prior to the 1992 eruption increased to 1.2 dropping quickly below 1.0 without forming a clear minimum (cf. Fig. 7b). The *b*-value variation during the 2004–2006 unrest has a similar shape to the one observed when deeper events were included in the estimation.

5. Robustness and sensitivity of *b*-value variation

It is generally recognized that the natural variability of *b*-values only partly results from physical causes, whereas another part can be attributed to factors related to the *b*-value estimation (Amorèse et al., 2010; Roberts et al., 2015; Nava et al., 2016; Marzocchi et al., 2019). These factors can be grouped in two categories depending on how significant is the bias that they incur to the estimated *b*-values. In the first category belong magnitude errors and magnitude binning, whose bias is either small or it can be removed. As already shown by Marzocchi et al. (2019), magnitude errors within reasonable bounds affect very little the estimation of *b*-values, while the effect of magnitude binning can be corrected by adding an appropriate term in the maximum likelihood estimator as has been done in this study (see section 3.1). The second category comprises the estimation method, the completeness magnitude and the truncation of the Gutenberg-Richter relationship, all of which may incur a significant bias that can artificially increase the *b*-value variability. This category is the most important, since the bias incurred by these factors can be minimized but cannot be completely removed.

The application of least-squares regression is a well-known source of bias when estimating *b*-values and their uncertainties (Sandri and

Table 2
Summary of the comparison between *b*-values estimated using the Aki-Utsu (AU) and Tinti-Mulargia (TM) method for each volcano. The quantity $<b_{AU} - b_{TM}>$ represents the mean difference, $<\delta b_{AU}>$ and $<\delta b_{TM}>$ are the mean uncertainties of the two estimates, and $\tilde{b}_{AU}$, $\tilde{b}_{TM}$ are the median *b*-values.

Volcano	$<b_{AU} - b_{TM}>$	$<\delta b_{AU}>$	$<\delta b_{TM}>$	$\tilde{b}_{AU}$	$\tilde{b}_{TM}$
Makushin	3.27×10^{-3}	0.02	0.03	0.74	0.73
Martin	-3.19×10^{-3}	0.03	0.03	0.75	0.76
Redoubt	0.06	0.04	0.05	1.00	0.89
Spurr (≤ 40 km)	4.93×10^{-3}	0.03	0.05	0.99	1.00
Spurr (≤ 12 km)	0.02	0.04	0.06	1.02	1.01

Marzocchi, 2007), prompting authors to use the Aki-Utsu method instead, an approach also adopted in this study. However, another method for estimating *b*-values was suggested by Tinti and Mulargia (1987) where the *b*-value is expressed as

$$b_{TM} = \frac{1}{\delta M ln10} ln\left(1 + \frac{\delta M}{< M > - M_c}\right) \quad (5)$$

Even though very few studies have tried to compare the *b*-values estimated by these two methods (for an exception see Shelly et al., 2016), it is generally assumed that both of them produce similar results. In order to check this, the *b*-values for each volcano have been recalculated following the same procedure as described previously, this time using Eq. (5). The results were plotted in the same way as before and are included as Figs. S1-S4 in the supplementary material that accompanies this work. Table 2 reports the mean difference of the two *b*-value estimates (i.e $<b_{AU} - b_{TM}>$) at each volcano and compares this with the corresponding mean bootstrap uncertainties. As it can be seen, at three of the volcanoes the difference is one order of magnitude smaller than the mean uncertainties, hence it can be concluded that the estimation method did not introduce any significant bias. The mean difference is more significant in the case of Redoubt and less so for the case of shallow seismicity beneath Spurr. A look at the temporal variation of b_{TM} for these two cases (Figs. S3 and S4b) does indicate differences when compared to the variations of b_{AU}, especially during the eruptive periods of 1989–1992. However, the general pattern of *b*-value variation remains the same independently of which estimation method was employed.

The two other factors, namely completeness magnitude and the truncation of the Gutenberg-Richter relationship, strongly depend on the size of the estimation window and its time span. The size of the selected window is connected to the temporal variation of the completeness magnitude, with a larger window size providing a smoother variation of M_c as shown in Figs. 4–7. On the other hand, the use of MBC minimizes the bias caused by the truncation of the Gutenberg-Richter relationship by increasing the magnitude bandwidth for the majority of the windows. In order to assess the impact of a smaller window size on the variability of the *b*-values, the Aki-Utsu method is repeated for a window size of 200 events, rejecting windows that contained less than 100 events above the completeness magnitude. Figs. S5-S8 in the supplementary material depict the variation of M_c and *b*-values for this smaller window size at the four volcanoes under study. The results show that not only are the bootstrap uncertainties significantly larger, but also that M_c varies strongly with time, most likely due to the difficulty of maintaining the seismic networks fully operational during periods of severe weather. The variation of the *b*-values mirrors that of M_c with strong oscillations and with *b*-values reaching 1.5 or higher (see Figs. S7–S8). Such high *b*-values are probably biased due to the limited magnitude bandwidth of these windows (≤ 1.5). It can be concluded therefore that a smaller window size is more exposed to all the biases mentioned earlier, leading to an artificial increase of *b*-value variability and making any interpretation in terms of physical processes uncertain.

While this work was under review, Geffers et al. (2022) published a study where the authors utilized synthetic and real catalogs in order to investigate different biases in the estimation of *b*-values. Their study showed that a sample size of at least 1000 earthquakes and magnitude bandwidth (or 'dynamic range' according to Geffers et al.) above 1.5 are necessary for an accurate estimate of the *b*-value. Geffers et al. (2022) also found that in volcanic areas *b*-values are usually biased towards values above 1.2 due to the small catalog sizes used and the limited bandwidth. The authors finally recommended that estimations of *b*-values should also report the sample size used, magnitude bandwidth and completeness magnitude in order for one to judge their reliability. In agreement with Geffers et al. (2022), this study highlighted the same factors as sources of bias in *b*-value estimation and suggested ways to minimize them (such as MBC), as well as included the magnitude bandwidth information in the representation of the results (as in Figs. 4-7).

6. Discussion

In recent years there has been a large number of studies describing laboratory experiments that test the mechanical behavior and failure of different types of volcanic rocks (for an extensive review see Heap and Violay, 2021) with the aim of understanding seismicity rates and *b*-value variation at volcanoes. As mentioned previously, the inverse relationship between stress and the resulting *b*-value has been well-established in tectonic environments, however, additional factors have to be considered at volcanoes such as the presence of fluids, and the variable degree of heterogeneity of volcanic rocks. The results presented in this study highlight two important characteristics: first, the drop in *b*-values prior to eruption or unrest and second, the differences in the absolute level of *b*-value for some volcanoes, that may be either below or above 1.0 as implied by the median *b*-values shown in Table 2. These characteristics and their interpretation are directly linked to any attempt to incorporate *b*-value variation into existing volcano monitoring and alert schemes.

Smith et al. (2009) have tested the mechanical behavior of porphyritic andesite from Mount Shasta deformed under conditions prevalent in volcanic systems prior to eruptions (strain rate 10^{-5} s^{-1}, pressure up to 50 MPa, temperature up to 900 °C). As the sample was being deformed Acoustic Emissions (AE) were also recorded in order to be utilized as an analog for earthquakes and for reconstructing their frequency-magnitude distribution. The *b*-values of AE were estimated as a function of time for the different stages of deformation showing that the lowest *b*-value occurred just prior to sample failure. Similar results have been obtained after testing various samples of porphyritic dacite (Kendrick et al., 2021), lava dome andesite (Lavallée et al., 2013), or andesitic lava (Heap et al., 2014), utilizing again recordings of AE during the deformation and failure of the samples. All studies have interpreted these observations as a result of an increase in stress intensity at the tip of microcracks that eventually grow and coalesce into a large macroscopic fracture. The observed lowest *b*-values at the four Alaskan volcanoes coincide with the approximate timing of eruptions (Redoubt, Spurr), or with unrest (Makushin, Martin). An interpretation of these observations in the context of the laboratory experiments would thus suggest that the stress generated by shallow intrusions and exsolution of magmatic fluids, initially produces numerous small cracks that progressively coalesce into a macroscopic fracture. This fracture subsequently becomes the conduit for fluid transport that may either propagate to the surface leading to an eruption, or its propagation is arrested causing only unrest.

Another set of laboratory experiments have investigated the effect of material heterogeneity on crack development and failure of volcanic rocks as well as on the estimated *b*-values. Vasseur et al. (2015) used synthetic, sintered glass samples that mimicked the natural heterogeneity of volcanic rocks by exhibiting a variable degree of porosity (for the use of porosity as a proxy for heterogeneity see also Heap et al., 2014). At this point it should be mentioned that Kendrick et al. (2021)

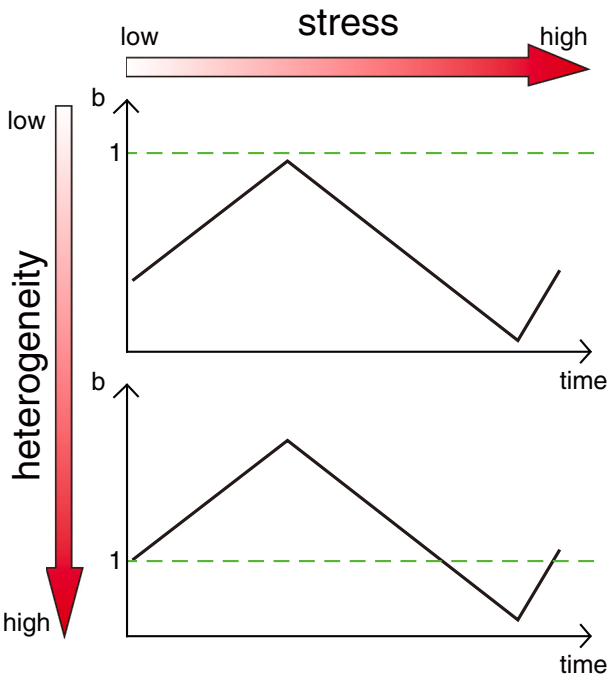

Fig. 8. Cartoon that summarizes the main conclusions of this work in terms of the time evolution of the *b*-value as a function of increasing stress and material heterogeneity.

generalized the notion of heterogeneity to include not only total porosity but also crystal size, geometry and distribution. The results of these experiments showed that cracks propagated over small distances in heterogeneous samples generating localized fracturing, while in less heterogeneous samples cracks propagated to large distances precipitating in this way a catastrophic system failure. In terms of *b*-values estimated using AE recordings, it was found that less heterogeneous samples exhibited *b*-values of 1.0 or lower, in contrast to the more heterogeneous ones where *b*-values were equal to 1.0 or higher. In this context, the observed difference in the *b*-values, which is expressed by the median *b*-values in Table 2, may reflect differences in the degree of rock heterogeneity. Hence *b*-values at Makushin and Martin are below unity representing less heterogeneous material, while at Spurr and Redoubt *b*-values are equal to 1.0 or higher indicating the presence of more significant heterogeneity. The cartoon in Fig. 8 illustrates the idea that at active volcanoes stress fluctuations determine the peaks and troughs of *b*-value variation, however, it is material heterogeneity at each individual volcano that determines the absolute values of this variation. The general applicability of this proposition needs to be confirmed by further studies at other active volcanoes around the world, that would also cover diverse volcanological and petrological types.

7. Conclusions

Similar to other geophysical parameters estimated from observed data, *b*-value estimation is sensitive to the quality and quantity of earthquake catalogs as well as to methodological biases. This study attempted to utilize catalog data of several years duration in order to estimate the long-term variation of *b*-value at 4 selected Alaskan volcanoes and to minimize known biases that could contaminate the resulting variations. The main conclusions of this work are as follows:

- The use of MBC provides an objective way to choose the window size for calculating *b*-values as a function of time by reducing the bias imposed by a truncated Gutenberg-Richter distribution. When MBC is combined with the *b*VS method it is also possible to minimize the effect of the spatio-temporal heterogeneity of the completeness magnitude. This may be especially important for catalogs compiled using seismic networks that are exposed to severe weather conditions, or are installed in remote and difficult to access areas like the Aleutian islands. This methodology could also be useful in the reconstruction of *b*-value variation for non-volcanic earthquake swarms, as for example in the case of induced seismicity in exploited geothermal fields.
- Periods of decreasing *b*-values at the four Alaskan volcanoes under study coincide with periods leading up to eruptions (Redoubt, Spurr) or unrest (Makushin, Martin). This agrees well with previously published laboratory experiments indicating that volcanic rocks under increasing stress form numerous microcracks that eventually coalesce into a large macroscopic fracture prior to failure. Such a fracture in a volcanological setting may then act as a conduit for transporting magmatic fluids to the surface.
- Throughout the time period considered, Makushin and Martin exhibited *b*-values below unity, while Redoubt and Spurr registered *b*-values around 1.0 or higher. This difference can be explained as a result of the variable degree of heterogeneity at each volcano and puts forward the proposition that stress level determines the minimum and maximum *b*-values, whereas material heterogeneity likely affects the absolute values of this variation.

Declaration of Competing Interest

The author declares that there is no competing financial interests or personal relationships that could have appeared to influence the work reported in this paper.

Acknowledgments

This research has been supported by a grant provided by the Ministry Of Science and Technology (MOST) of Taiwan. The AVO catalog (1989–2017) that has been used in this work is freely available as part of the electronic supplement that accompanies the report of Power et al. (2019). All other material can be obtained from the author upon reasonable request. I would like to thank Ed Llewellin for the editorial handling of the manuscript and two anonymous reviewers for their helpful comments.

Appendix A. Supplementary data

Supplementary data to this article can be found online at https://doi.org/10.1016/j.jvolgeores.2022.107572.

References

Aki, K., 1965. Maximum likelihood estimate of *b* in the formula logN = a-bM and its confidence limits. Bull. Earthq. Res. Inst., Univ. Tokyo 43, 237–239.
Amorèse, D., Grasso, J.-R., Rydelek, P.A., 2010. On the varying *b*-values with depth: results from computer-intensive tests for southern California. Geophys. J. Int. 180, 347–360. https://doi.org/10.1111/j.1365-246X.2009.04414.x.
Bridges, D.L., Gao, S.S., 2006. Spatial variation of seismic *b*-values beneath Makushin volcano, Unalaska island, Alaska. Earth Planet. Sci. Lett. 245, 408–415. https://doi.org/10.1016/j.epsl.2006.03.010.
Bull, K.F., Buurman, H., 2013. An overview of the 2009 eruption of Redoubt volcano, Alaska. J. Volcanol. Geotherm. Res. 259, 2–15. https://doi.org/10.1016/j.jvolgeores.2012.06.024.
Buurman, H., West, M.E., Thompson, G., 2013. The seismicity of the 2009 Redoubt eruption. J. Volcanol. Geotherm. Res. 259, 16–30. https://doi.org/10.1016/j.jvolgeores.2012.04.024.
Buurman, H., Nye, C.J., West, M.E., Cameron, C., 2014. Regional controls on volcano seismicity along the Aleutian arc. Geophys. Geochem. Geosyst. 15, 1147–1163. https://doi.org/10.1002/2013GC005101.
Cameron, C.E., Prejean, S.G., Coombs, M.L., Wallace, K.L., Power, J.A., Roman, D.C., 2018. Alaska volcano observatory alert and forecasting timeliness: 1989-2017. Front. Earth Sci. 6, 86. https://doi.org/10.3389/feart.2018.00086.
Chiba, K., Shimizu, H., 2018. Spatial and temporal distributions of *b*-value in and around Shinmoe-dake, Kirishima volcano, Japan. Earth Planets Space 70, 122. https://doi.org/10.1186/s40623-018-0892-7.

Doukas, M.P., McGee, K.A., 2007. A compilation of gas emission rate data from volcanoes of Cook inlet (Spurr, Crater Peak, Redoubt, Iliamna and Augustine) and Alaska peninsula (Douglas, Fourpeaked, Griggs, Mageik, Martin, Peulik, Ukinrek Maars, and Veniaminof), Alaska from 1995 to 2006, USGS Open-File Report 2r007–1400.

El-Isa, Z.H., Eaton, D.W., 2014. Spatiotemporal variations in the *b*-value of earthquake magnitude-frequency distributions: Classifications and causes. Tectonophysics 615-616, 1–11. https://doi.org/10.1016/j.tecto.2013.12.001.

Farrell, J., Husen, S., Smith, R.B., 2009. Earthquake swarm and *b*-value characterization of the Yellowstone volcano-tectonic system. J. Volcanol. Geotherm. Res. 188, 260–276. https://doi.org/10.1016/j.jvolgeores.2009.08.008.

Geffers, G.-M., Main, I.G., Naylor, M., 2022. Biases in estimating *b*-values from small earthquake catalogues: how high are high *b*-values. Geophys. J. Int. 229, 1840–1855, 10.1093/gji/ggac028.

Global Volcanism Program, 1995a. Report on Makushin (United States) (Wunderman, R., ed.). Bulletin of the Global Volcanism Network, 20:1. Smithsonian Institution. https://doi.org/10.5479/si.GVP.BGVN199501-311310.

Global Volcanism Program, 1995b. Report on Martin (United States) (Wunderman, R., ed.). Bulletin of the Global Volcanism Network, 20:3. Smithsonian Institution. https://doi.org/10.5479/si.GVP.BGVN199503-312140.

Global Volcanism Program, 2001. Report on Makushin (United States) (Wunderman, R., ed.). Bulletin of the Global Volcanism Network, 26:6. Smithsonian Institution. https://doi.org/10.5479/si.GVP.BGVN200106-311310.

Global Volcanism Program, 2012. Report on Martin (United States) (Dennen, R., and Wunderman, R., eds.). Bulletin of the Global Volcanism Network, 37:1. Smithsonian Institution. https://doi.org/10.5479/si.GVP.BGVN201201-312140.

Global Volcanism Program, 2020. Report on Makushin (United States). In: Sennert, S.K. (Ed.), Weekly Volcanic Activity Report, 24 June-30 June 2020. Smithsonian Institution and US Geological Survey.

Goebel, T.H.W., Kwiatek, G., Becker, T.W., Brodsky, E.E., Dresen, G., 2017. What allows seismic events to grow big?: Insights from *b*-value and fault roughness analysis in laboratory stick-slip experiments. Geology 45, 815–818. https://doi.org/10.1130/G39147.1.

Gulia, L., Tormann, T., Wiemer, S., Herrmann, M., Seif, S., 2016. Short-term probabilistic earthquake risk assessment considering time-dependent *b* values. Geophys. Res. Lett. 43, 110–1108. https://doi.org/10.1002/2015GL066686.

Gutenberg, B., Richter, C., 1944. Frequency of earthquakes in California. Bull. Seismol. Soc. Am. 34, 185.

Heap, M.J., Violay, M.E.S., 2021. The mechanical behaviour and brittle failure modes of volcanic rocks: a review. Bull. Volcanol. 83, 33. https://doi.org/10.1007/s00445-021-01447-2.

Heap, M.J., Lavallée, Y., Petrakova, L., Baud, P., Reuschlé, T., Varley, N.R., Dingwell, D. B., 2014. Microstructural controls on the physical and mechanical properties of edifice-forming andesites at Volcán de Colima, Mexico. J. Geophys. Res. Solid Earth 119 (4), 2925–2963. https://doi.org/10.1002/2013JB010521.

Hong, T.-K., Houng, S.-E., Jo, E., 2014. Temporal changes of medium properties during explosive volcanic eruption. Geophys. Res. Lett. 41 https://doi.org/10.1002/2014GL059408.

Ishimoto, M., Iida, K., 1939. Observations of earthquakes registered with the microseismograph constructed recently. Bull. Earthquake Res. Inst. 17, 443–478.

Kasatkina, E., Kulakov, I., West, M., Izbekov, P., 2014. Seismic structure beneath Redoubt volcano during the 2009 eruption inferred from local earthquake tomography. J. Geophys. Res. Solid Earth 119, 4938–4954. https://doi.org/10.1002/2013JB010935.

Kendrick, J.E., Schaefer, L.N., Schauroth, J., Bell, A.F., Lamb, O.D., Lamur, A., Miwa, T., Coats, R., Lavallée, Y., Kennedy, B.M., 2021. Physical and mechanical rock properties of a heterogeneous volcano: the case of Mount Unzen. Solid Earth 12, 633–664. https://doi.org/10.5194/se-12-633-2-2021.

Kulakov, I., Smirnov, S.Z., Gladkov, V., Kasatkina, E., West, M., El Khrepy, S., Al-Arifi, N., 2018. Causes of volcanic unrest at Mt Spurr in 2004-2005 inferred from repeated tomography. Sci. Rep. 8, 17482. https://doi.org/10.1038/s41598-018-35453-w.

Lanza, F., Thurber, C.H., Syracuse, E.M., Power, J.A., Ghosh, A., 2020. Seismic tomography of compressional wave velocity and attenuation structure for Makushin volcano, Alaska. J. Volcanol. Geotherm. Res. 393, 106804 https://doi.org/10.1016/j.volgeores.2020.106804.

Lanza, F., Roman, D.C., Power, J.A., Thurber, C.H., Hudson, T., 2022. Complex magmatic-tectonic interactions during the 2020 Makushin volcano, Alaska, earthquake swarm. Earth Planet. Sci. Lett. 587, 117538. https://doi.org/10.1016/j.epsl.2022.117538.

Lavallée, Y., Benson, P.M., Heap, M.J., Hess, K.U., Flaws, A., Schillinger, B. Meredith P. G., Dingwell, D.B., 2013. Reconstructing magma failure and the degassing network of dome-building eruptions. Geology 41 (4), 515–518. https://doi.org/10.1130/G33948.1.

Lopez, T., Tassi, F., Aiuppa, A., Galle, B., Rizzo, A.L., Fiebig, J., Capecchiacci, F., Giudice, G., Caliro, S., Tamburello, G., 2017. Geochemical constraints on volatile sources and subsurface conditions at Mount Martin, Mount Mageik, and Trident volcanoes, Katmai volcanic cluster, Alaska. J. Volcanol. Geotherm. Res. 347, 64–81. https://doi.org/10.1016/j.volgeores.2017.09.001.

Lu, Z., Dzurisin, D., 2014. InSAR Observations and Insights into Aleutian Volcanism, InSAR Imaging of Aleutian Volcanoes. Springer-Berlin, Heidelberg, pp. 347–363.

Marzocchi, W., Sandri, L., 2003. A review and new insights on the estimation of the *b*-value and its uncertainty. Ann. Geophys. 46, 1271–1282.

Marzocchi, W., Spassiani, I., Stallone, A., Taroni, M., 2019. How to be fooled searching for significant variations of the *b*-value. Geophys. J. Int. 220, 1845–1856. https://doi.org/10.1093/gji/ggz541.

Mignan, A., Woessner, J., 2012. Estimating the magnitude of completeness for earthquake catalogs. In: Community Online Resource for Statistical Seismicity Analysis. https://doi.org/10.5078/corssa-00180805.

Moran, S.C., 2003. Multiple seismogenic processes for high-frequency earthquakes at Katmai National Park, Alaska: evidence from stress tensor inversions of fault-plane solutions. Bull. Seismol. Soc. Am. 93, 94–108.

Murphy, R., Thurber, C., Prejean, S., Bennington, N., 2014. Three-dimensional seismic velocity structure and earthquake relocations at Katmai, Alaska. J. Volcanol. Geotherm. Res. 276, 121–131. https://doi.org/10.1016/j.volgeores.2014.02.022.

Murru, M., Montuori, C., Wyss, M., Privitera, E., 1999. The locations of magma chambers at Mt Etna, Italy, mapped by *b*-values. Geophys. Res. Lett. 26, 2253–2556.

Nava, F.A., Márquez-Ramírez, V.H., Zuniga, F.R., Ávila-Barrientos, L., Quinteros, C.B., 2016. Gutenberg-Richter *b*-value maximum likelihood estimation and sample size. J. Seismol. 21, 127–135. https://doi.org/10.1007/s10950-016-9589-1.

O'Brien, J.F., Roman, D.C., Dixon, J.P., Power, J.A., Arnold, R., 2012. Multiple causes for non-eruptive seismic swarms at Mt Martin, Katmai volcanic cluster, Alaska (2004-2008). J. Volcanol. Geotherm. Res. 229-230, 13–22. https://doi.org/10.1016/j.volgeores.2012.03.011.

Pesicek, J.D., Wellik, J.J., Prejean, S.G., Ogburn, S.E., 2018. Prevalence of seismic rate anomalies preceding volcanic eruptions in Alaska. Front. Earth Sci. 6, 100. https://doi.org/10.3389/feart.2018.00100.

Power, J.A., Jolly, A.D., Nye, C.J., Harbin, M.L., 2002. A conceptual model of the Mount Spurr magmatic system from seismic and geochemical observations of the 1992 Crater Peak eruption sequence. Bull. Volcanol. 64, 206–218.

Power, J.A., Stihler, S.D., Chouet, B.A., Haney, M.M., Ketner, D.M., 2013. Seismic observations of Redoubt Volcano, Alaska - 1989-2010 and a conceptual model of the Redoubt magmatic system. J. Volcanol. Geotherm. Res. 259, 31–44. https://doi.org/10.1016/j.volgeores.2012.09.014.

Power, J.A., Friberg, P.A., Haney, M.M., Parker, T., Stihler, S.D., Dixon, J.P., 2019. A unified catalog of earthquake hypocenters and magnitudes at volcanoes in Alaska - 1989 to 2018. In: U. S. Geological Survey Scientific Investigations Report 2019-5037, p. 17. https://doi.org/10.3133/sir20195037.

Power, J.A., Haney, M.M., Botnik, S.M., Dixon, J.P., Fee, D., Kaufman, A.M., Ketner, D. M., Lyons, J.J., Parker, T., Paskievitch, J.F., Read, C.W., Searcy, C., Stihler, S.D., Tepp, G., Welch, A.G., 2020. Goals and development of the Alaska Volcano observatory seismic network and application to forecasting and detecting volcanic eruptions. Seismol. Res. Lett. 91, 647–659. https://doi.org/10.1785/0220190216.

Roberts, N.S., Bell, A.F., Main, I.G., 2015. Are volcanic *b*-values high, and if so when? J. Volcanol. Geotherm. Res. 308, 127–141. https://doi.org/10.1016/j.jvolgeores.2015.10.021.

Roman, D., Cashman, K.V., 2006. The origin of volcano-tectonic swarms. Geology 34, 457–460. https://doi.org/10.1130/G22269.1.

Sammonds, P.R., Meredith, P.G., Main, I.G., 1992. Role of pore fluids in the generation of seismic precursors to shear fracture. Nature 359 (6392), 228–230.

Sandri, L., Marzocchi, W., 2007. A technical note on the bias in the estimation of the *b*-value and its uncertainty through the least squares technique. Ann. Geophys. 50, 329–339.

Scholz, C.H., 1968. The frequency-magnitude relation of microfracturing in rock and its relation to earthquakes. Bull. Seismol. Soc. Am. 58, 399–415.

Scholz, C.H., 2015. On the stress dependence of the earthquake *b* value. Geophys. Res. Lett. 42, 1399–1402. https://doi.org/10.1002/2014GL062863.

Schorlemmer, D., Wiemer, S., Wyss, M., 2005. Variations in earthquake-size distribution across different stress regimes. Nature 437, 539–542. https://doi.org/10.1038/nature04094.

Shelly, D.R., Ellsworth, W.L., Hill, D.P., 2016. Fluid-faulting evolution in high definition: Connecting fault structure and frequency-magnitude variations during the 2014 Long Valley Caldera, California, earthquake swarm. J. Geophys. Res. Solid Earth 121, 1776–1795. https://doi.org/10.1002/2015JB012719.

Smith, R., Sammonds, P.R., Kilburn, C.R.J., 2009. Fracturing of volcanic systems: Experimental insights into pre-eruptive conditions. Earth Planet. Sci. Lett. 280, 211–219. https://doi.org/10.1016/j.epsl.2009.01.032.

Syracuse, E.M., Maceira, M., Zhang, H., Zhang, C.H., 2015. Seismicity and structure of Akutan and Makushin volcanoes, Alaska, using joint body and surface wave tomography. J. Geophys. Res. Solid Earth 120, 1036–1052. https://doi.org/10.1002/2014JB011616.

Tibaldi, A., Bonali, F.L., 2017. Intra-arc and back-arc volcano-tectonics: Magma pathways at Holocene Alaska-Aleutian volcanoes. Earth Sci. Rev. 167, 1–26. https://doi.org/10.1016/j.earscirev.2017.02.004.

Tinti, S., Mulargia, F., 1987. Confidence intervals of *b* values for grouped magnitudes. Bull. Seismol. Soc. Am. 77, 2125–2134.

Utsu, T., 1965. A method for determining the value of *b* in a formula logn = a-bM showing the magnitude-frequency relation for earthquakes. Geophys. Bull. Hokkaido Univ. 13, 99–103.

Vasseur, J., Wadsworth, F.B., Lavallée, Y., Bell, A.F., Main, I.G., Dingwell, D.B., 2015. Heterogeneity: the key to failure forecasting. Sci. Rep. 5, 13259. https://doi.org/10.1038/srep13259.

Warren, N., Latham, C., 1970. An experimental study of thermally induced microfracturing and its relation to volcanic seismicity. J. Geophys. Res. 75, 4455–4464.

Wei, S.S., Ruprecht, P., Gable, S.L., Huggins, E.G., Ruppert, N., Gao, L., Zhang, H., 2021. Along-strike variations in intermediate-depth seismicity and arc magmatism along the Alaska Peninsula. Earth Planet. Sci. Lett. 563, 116878 https://doi.org/10.1016/j.epsl.2021.116878.

White, R.A., McCausland, W., 2019. A process-based model of pre-eruption seismicity patterns and its use for eruption forecasting at dormant stratovolcanoes. J. Volcanol. Geotherm. Res. 382, 267–297, 10.1016/j.jvolgeores.2019.03.004.

Wiemer, S., McNutt, S.R., Wyss, M., 1998. Temporal and three-dimensional spatial analyses of the frequency-magnitude distribution near Long Valley Caldera, California. Geophys. J. Int. 134, 409–421.
Wiemer, S., Wyss, M., 2000. Minimum magnitude of complete reporting in earthquake catalogs: examples from Alaska, the Western United States, and Japan. Bull. seism. Soc. Am. 90, 859–869.
Wilson, L., Parfitt, E., 2008. Fundamentals of Volcanology. Blackwell Publishing.
Woessner, J., Wiemer, S., 2005. Assessing the quality of earthquake catalogues: estimating the magnitude of completeness and its uncertainty. Bull. Seismol. Soc. Am. 95, 684–698. https://doi.org/10.1785/0120040007.
Wyss, M., Shimazaki, K., Wiemer, S., 1997. Mapping active magma chamber by *b* values beneath the off-Ito volcano, Japan. J. Geophys. Res. 102, 20,413-20,422.
Wyss, M., Klein, F., Nagamine, K., Wiemer, S., 2001. Anomalously high *b*-values in the South Flank of Kilauea volcano, Hawaii: evidence for the distribution of magma below Kilauea's East rift zone. J. Volcanol. Geotherm. Res. 106, 23–37.